Downslope Windstorms of San Diego County. Part II: Physics Ensemble Analyses and Gust Forecasting

YANG CAO

Atmospheric Data Solutions, LLC, Santa Ana, California

ROBERT G. FOVELL

Department of Atmospheric and Environmental Sciences, University at Albany, State University of New York, Albany, New York

(Manuscript received 27 November 2017, in final form 30 January 2018)

ABSTRACT

The ‘‘Santa Ana’’ winds of Southern California represent a high-impact weather event because their dry, fast winds can significantly elevate the wildfire threat. This high-resolution numerical study of six events of moderate or greater strength employs physics parameterization and stochastic perturbation ensembles to determine the optimal model configuration for predicting winds in San Diego County, with verification performed against observations from the San Diego Gas and Electric (SDG&E) mesonet. Results demonstrate model physics can have a material effect on the strength, location, and timing of the winds, with the land surface model playing an outsized role via its specification of surface roughness lengths. Even when bias in the network-averaged sustained wind forecasts is minimized, systematic biases remain in that many stations are consistently over- or underforecasted. The argument is made that this is an ‘‘unavoidable’’ error that represents localized anemometer exposure issues revealed through the station gust factor. A very simple gust parameterization is proposed for the mesonet based on the discovery that the network-averaged gust factor is independent of weather conditions and results in unbiased forecasts of gusts at individual stations and the mesonet as a whole. Combined with atmospheric humidity and fuel moisture information, gust forecasts can help in the assessment of wildfire risks.

The first objective of this paper is to further investigate the sensitivity of the intensity, spatial extent, and structure of these windstorms to model physics, and to explain why some LSMs outperformed others. This will be done by examining additional Santa Ana events that have occurred since the deployment of the SDG&E mesonet. The second is to develop a strategy for parameterizing small-scale wind gusts, which cannot be resolved in mesoscale models. This is motivated by the fact that gusts can cause an enormous amount of damage to electrical infrastructure.

Gustiness is a remarkable feature of many downslope windstorms (e.g., Durran 2003; Jackson et al. 2013). As an example, the well-studied 11 January 1972 Boulder, Colorado, downslope windstorm had wind bursts as high as $60\,\mathrm{m\,s^{-1}}$ (e.g., Klemp and Lilly 1975). Empirical and heuristic attempts have been made to estimate wind gusts by multiplying the resolved-scale sustained wind speed by a gust factor [GF, the ratio of the peak wind speed of a given duration (gust) to the mean wind speed for a given averaging period] empirically determined from available observations (e.g., Mitsuta and Tsukamoto 1989) or adding a scalar value to the sustained wind, assuming a normal distribution of wind fluctuations (e.g., Wieringa 1973; Panofsky et al. 1977; Beljaars 1987). Brasseur (2001) pursued a gust parameterization based on physical considerations, reflecting boundary layer turbulence. In this work, we motivate a remarkably simple gust algorithm, which is shown to be skillful when applied to sustained wind forecasts for both individual SDG&E stations and the mesonet as a whole.

The organization of this manuscript is as follows. The available observations, model experimental design, and verification strategy are described in section 2. Model sensitivity to model physics, stochastic perturbations, and surface roughness is investigated in section 3. Section 4 presents an analysis of wind forecast bias for individual stations. A simple yet skillful gust parameterization for the SDG&E network is introduced in section 5, and the final section presents the summary.

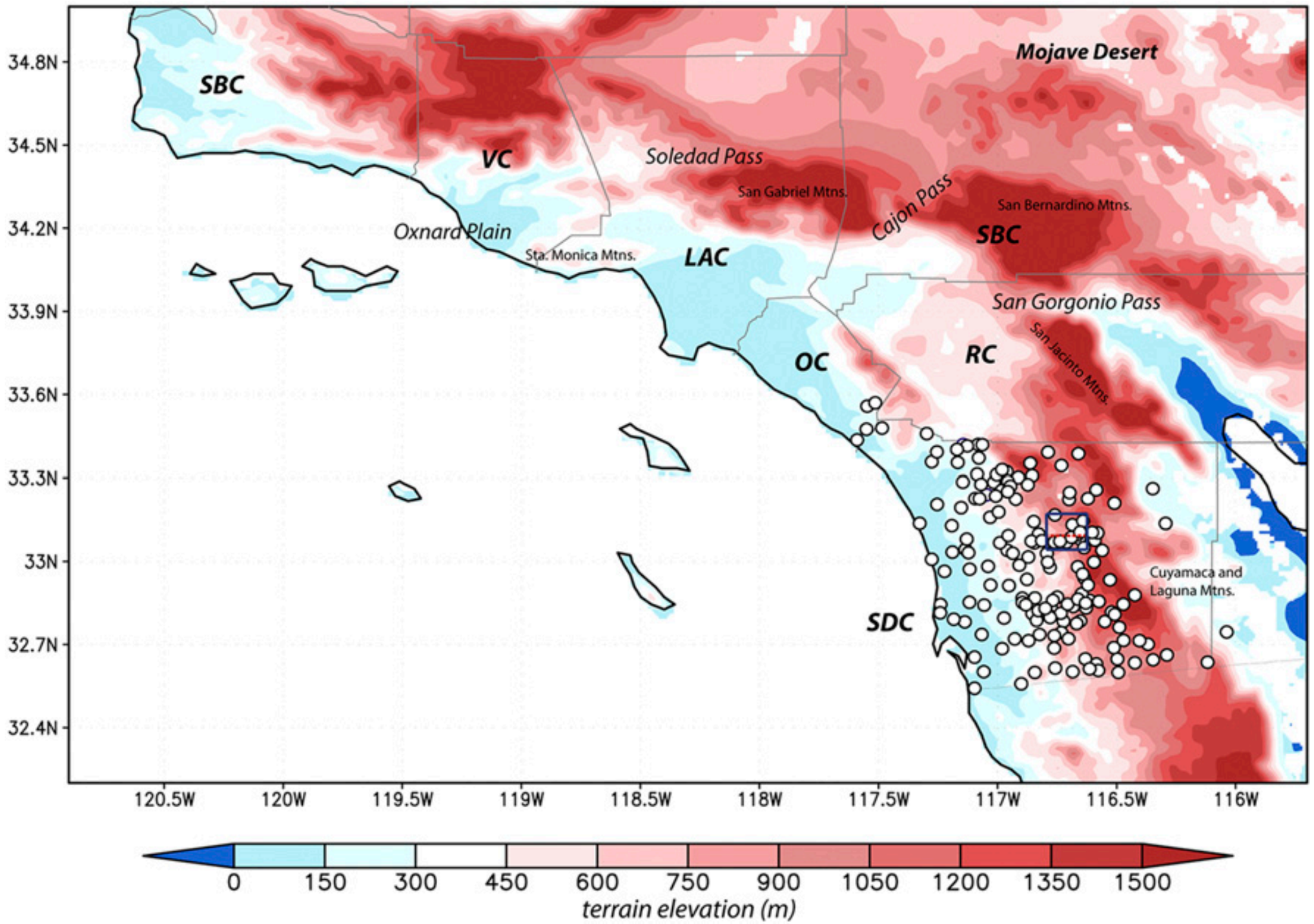

FIG. 1. Topography of Southern California (longitude on abscissa, latitude on ordinate), with selected place names. County outlines are in gray; identifiers are Santa Barbara (SBC), Ventura (VC), Los Angeles (LAC), Orange (OC), San Bernardino (SBC), and Riverside (RC) Counties. White dots denote SDG&E observational stations. The blue box highlights the Witch Creek region, and the red dashed line depicts the location of the vertical cross section across station WSY.

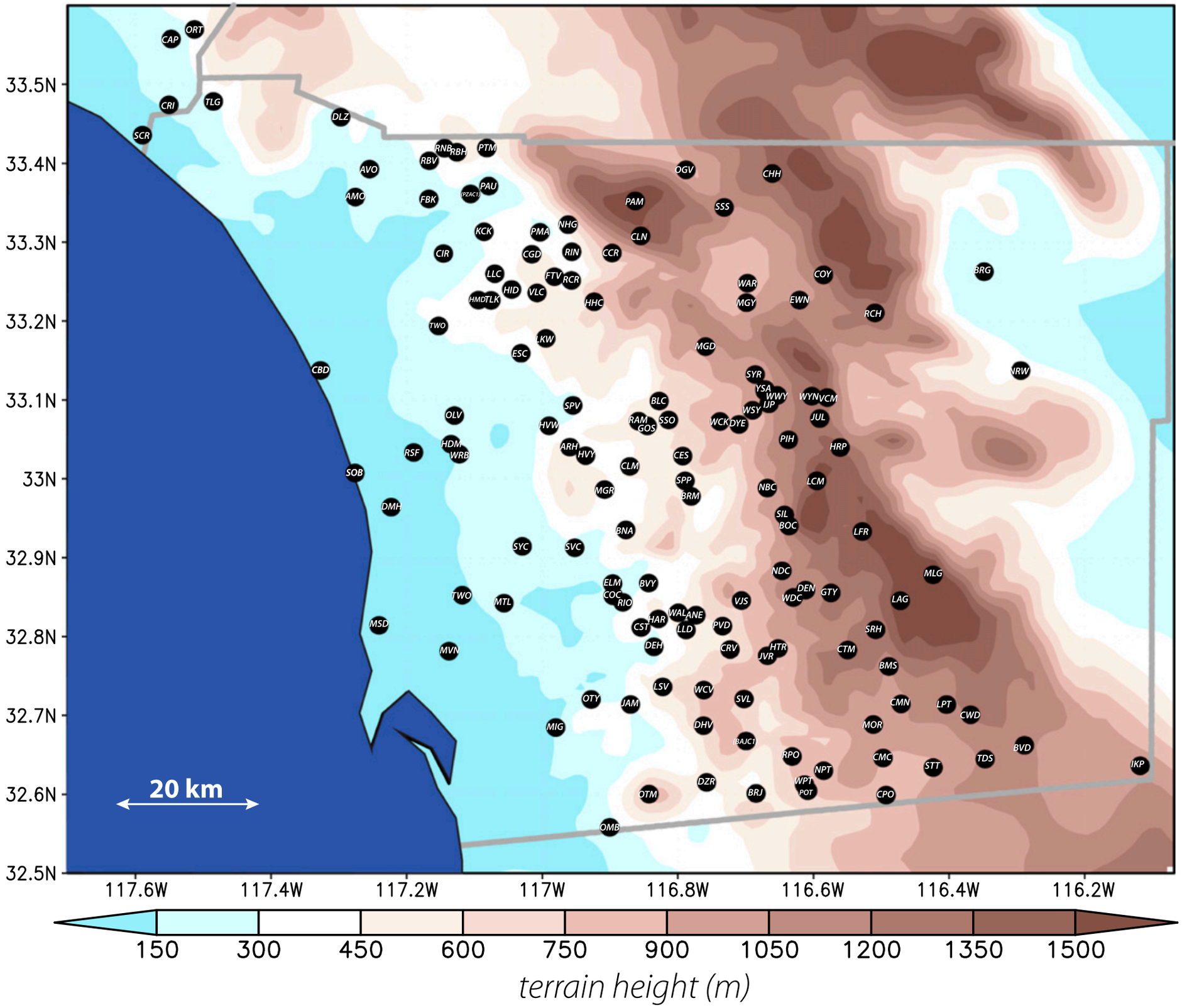

FIG. 1. SDG&E surface station locations (black dots), with underlying topography shaded. Station labels omit "SD" suffix. Stations were in place as of February 2013.

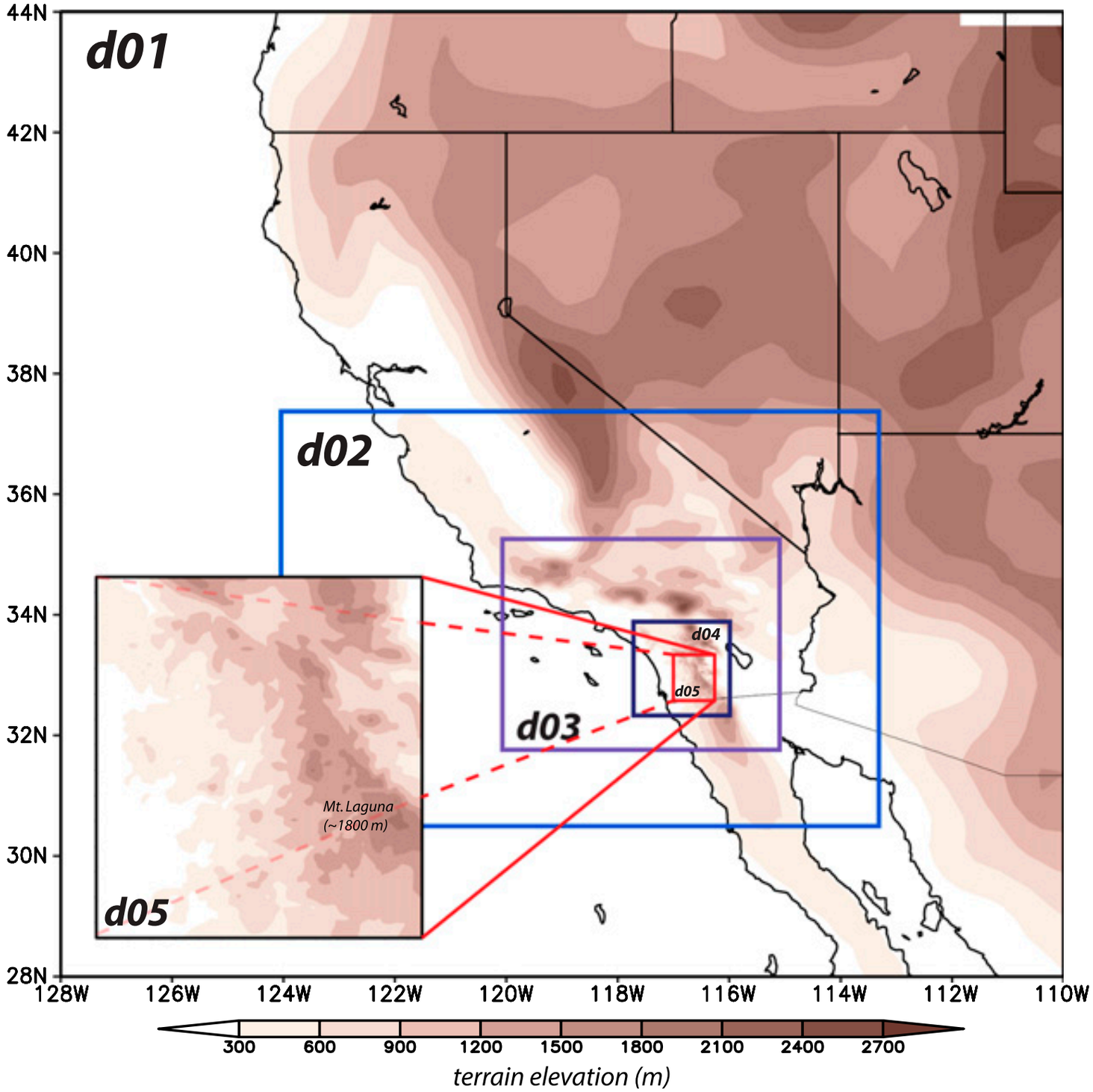

FIG. 3. Domain configuration for the WRF simulations, with topography shaded. Domains 1–5 employ horizontal grid spacings of 54, 18, 6, 2, and 0.667 km over Southern California, respectively. The inset shows an enlarged version of domain 5.

TABLE 1. Santa Ana wind events studied and their model initialization time. Here, Y denotes the event was used to create a physics ensemble and N denotes the event was not used for creating a physics ensemble.

Event	Initialization time and date	Used in the physics ensemble?
14–16 Feb 2013	1200 UTC 14 Feb	Y
4–6 Oct 2013	0600 UTC 3 Oct	Y
29 Apr–1 May 2014	0600 UTC 29 Apr	N
13–15 May 2014	0600 UTC 13 May	Y
23–25 Jan 2015	1200 UTC 23 Jan	N
11–13 Feb 2015	1200 UTC 11 Feb	N

Physics ensembles consisted of combinations of 5 land surface models (LSM) and 10 boundary layer (PBL) schemes.

3. Sensitivity tests: Model physics, stochastic perturbations, and surface roughnesses

a. February 2013 event physics ensemble

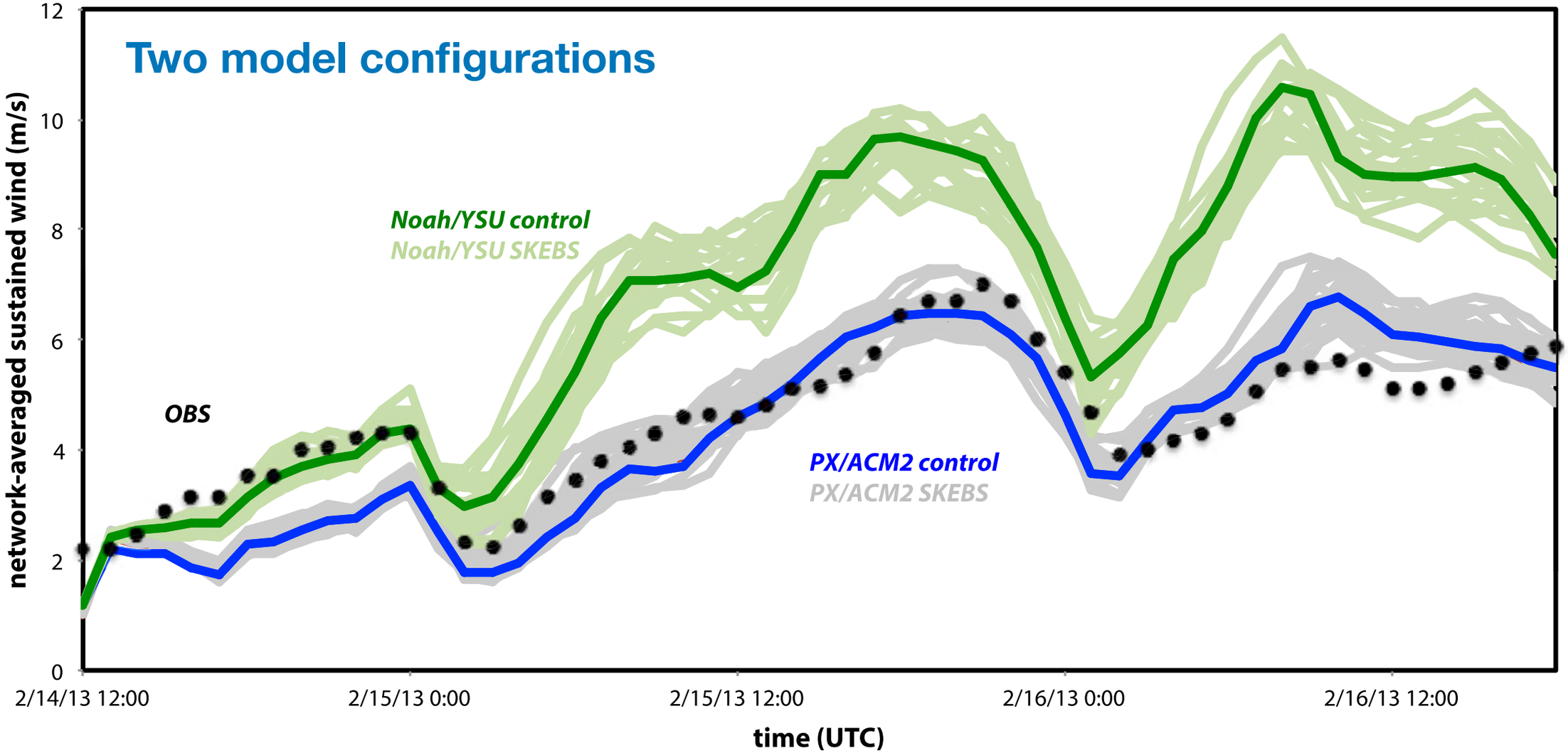

FIG. 2. Time series of network-averaged observed (black dots) and predicted (blue, PX–ACM2 control run; green, Noah–YSU control run) 6.1-m sustained winds ($m\,s^{-1}$) for the 14–16 Feb 2013 event. The gray and light green plumes reveal the ensemble spread created via SKEBS perturbations.

Four model configurations

wind speed (shaded contours), potential temperature (thick black contours)

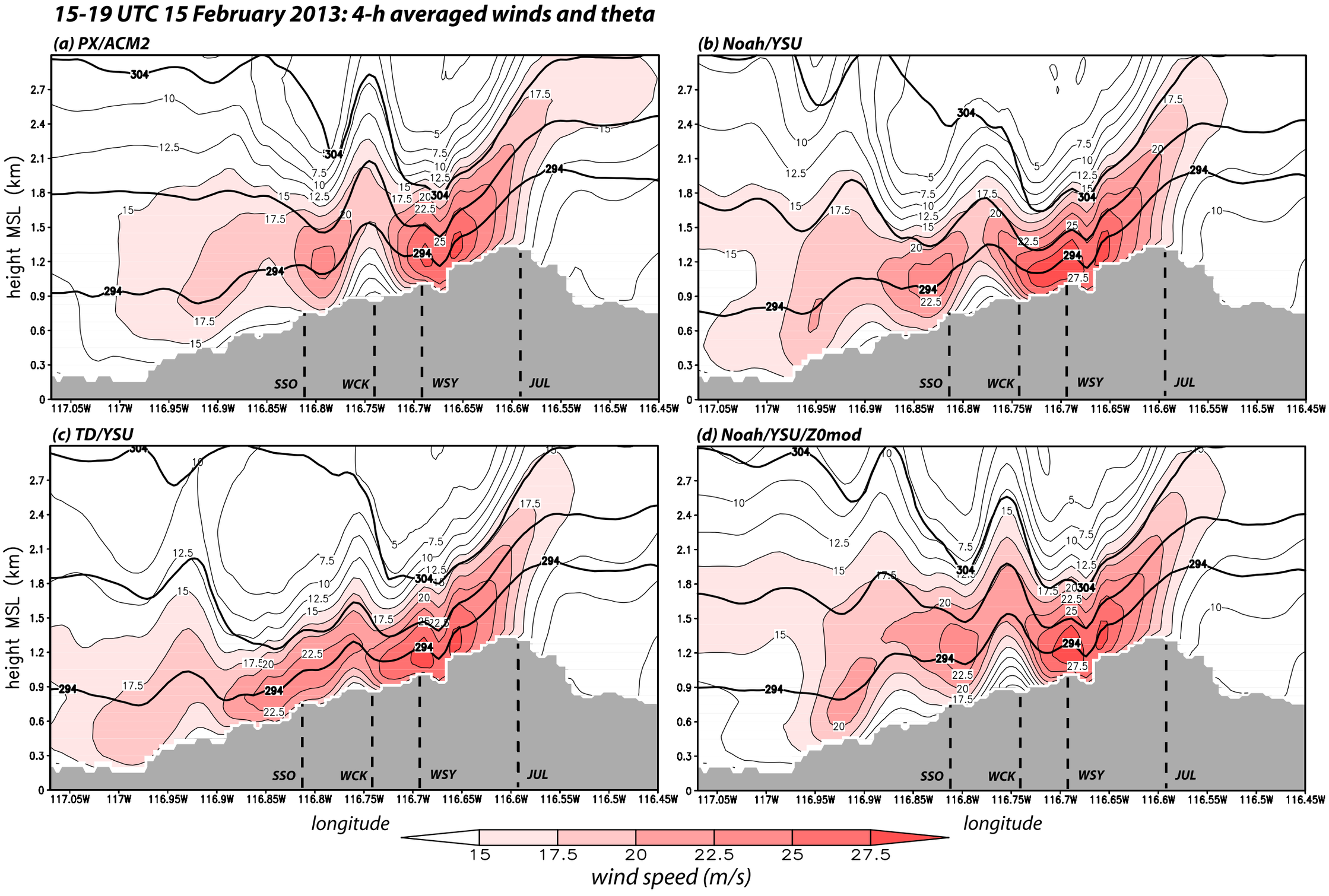

FIG. 3. Vertical cross sections of 4-h averaged horizontal wind speed (2.5 m s^{-1} contours and red shaded fields) and potential temperature (thick black 5-K contours) for the 1500–1900 UTC 15 Feb 2013 event, taken west–east across station WSY for four physics combinations: (a) PX–ACM2, (b) Noah–YSU, (c) TD–YSU, and (d) Noah–YSU–$z_0$mod.

b. Sensitivity to model random perturbations (February 2013 and May 2014 events)

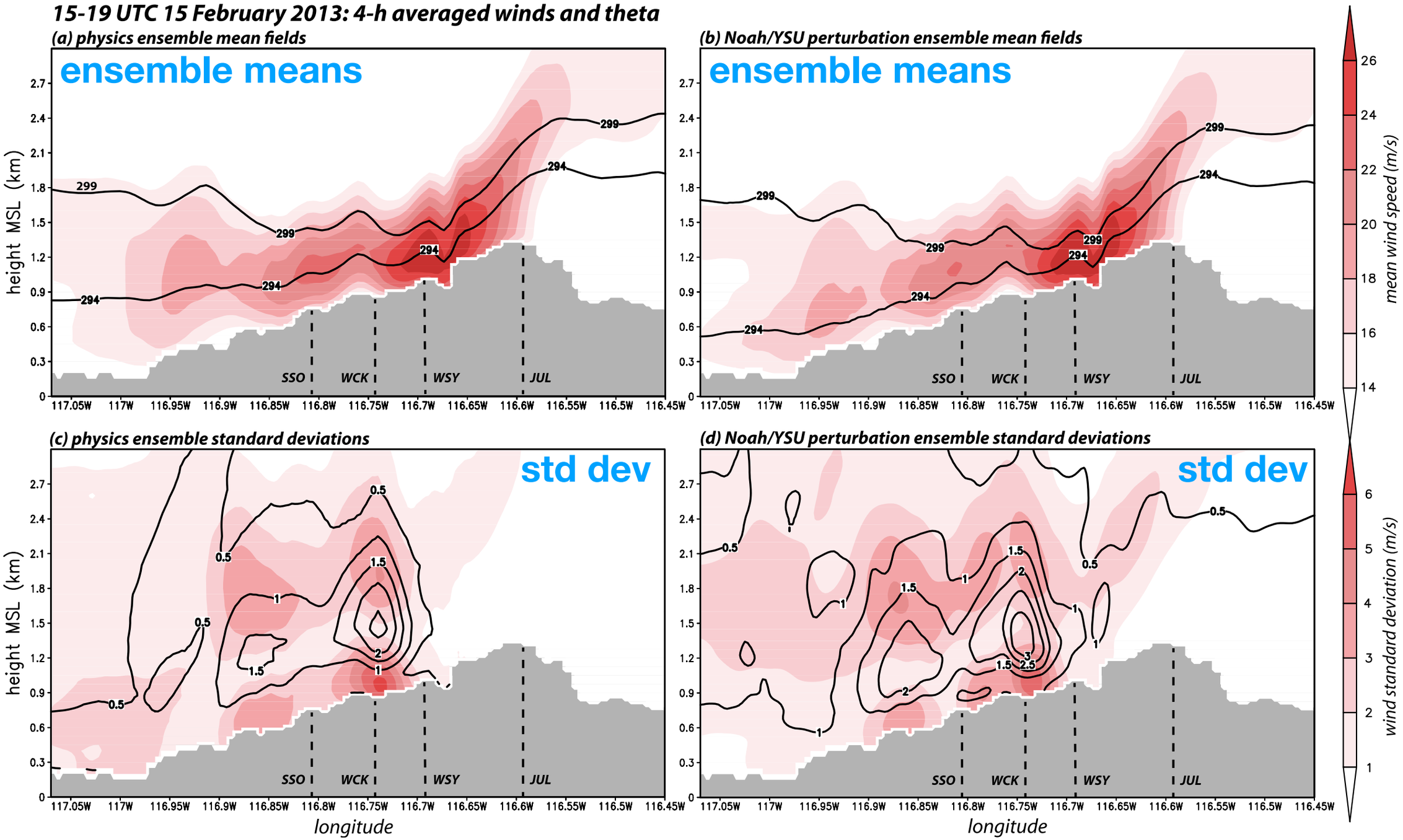

FIG. 4. As in Fig. 3, but for (a) the physics and (b) Noah–YSU perturbation ensembles' mean horizontal wind speed (shaded; m s^{-1}) and potential temperature (contoured; K) fields, and (c) the physics and (d) Noah–YSU perturbation ensembles' horizontal wind speed (shaded; m s^{-1}) and potential temperature standard deviations (contoured; K).

Figures 4b and 4d show that, by itself, applying perturbations to a single physics member, Noah–YSU, for the February 2013 event, generated qualitatively and even quantitatively comparable variations in wind speed and potential temperature to those produced by the physics ensemble during the jump period. Like the physics ensemble as a whole, members in the Noah–YSU SKEBS collection included runs in which the jump was very pronounced and others in which it failed to form (Fig. 5b), such that the feature disappeared from the perturbation ensemble mean (Fig. 4b).

Feb 2013 and May 2014 events

10-m winds for each ensemble member

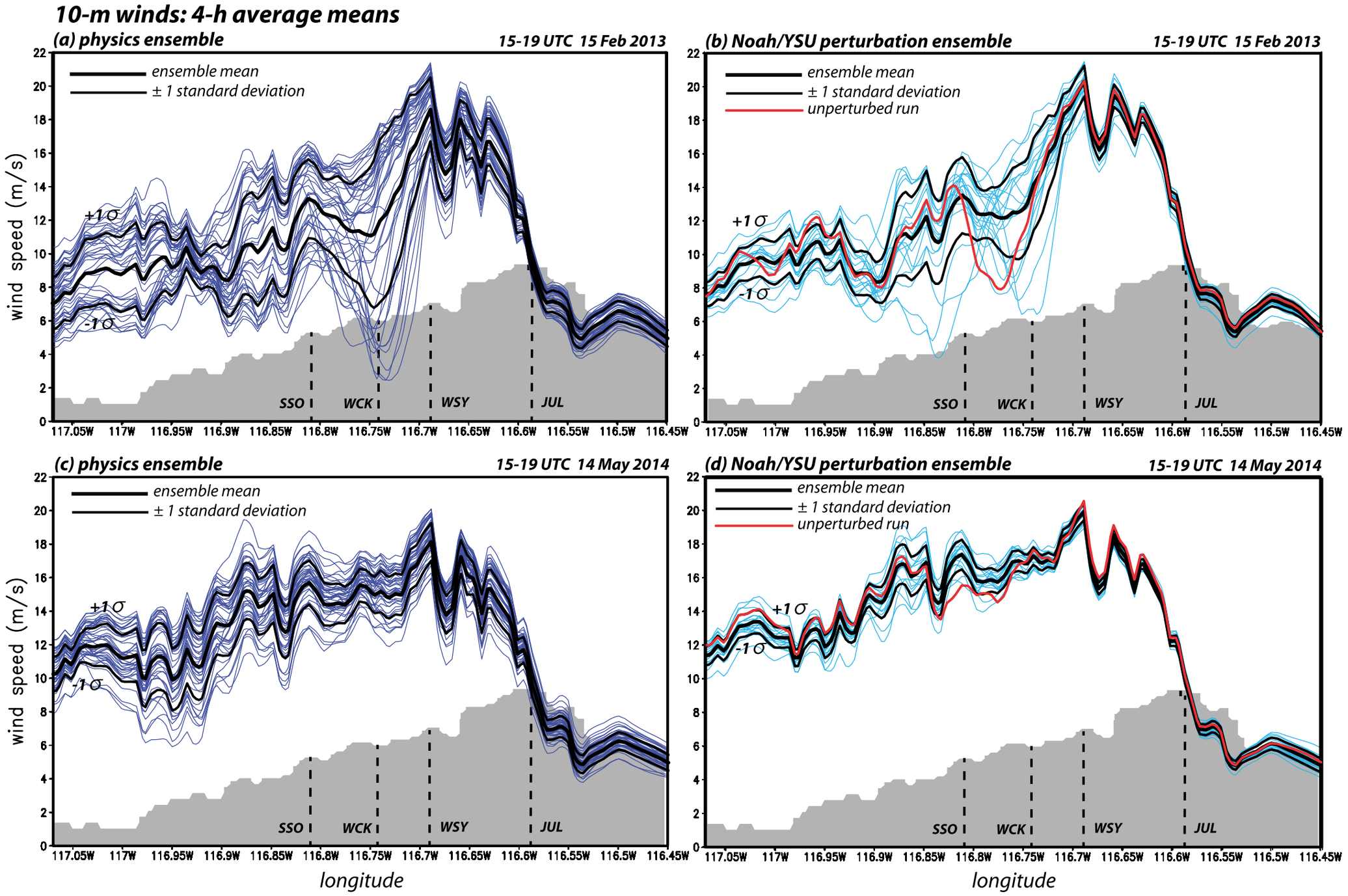

FIG. 5. Vertical cross sections taken west–east across WSY showing the ensemble mean (thick black line) and ±1 standard deviations (thin black lines) of the 4-h averaged horizontal 10-m wind speed (blue lines) for the first phase (1500–1900 UTC) of the 15 Feb 2013 event from the (a) physics and (b) Noah–YSU SKEBS ensembles. The same fields are also shown for the 1500–1900 UTC 14 May 2014 event from the (c) physics and (d) Noah/YSU SKEBS ensembles. The gray-shaded area depicts topography, shown for reference only. Approximate locations of some SDG&E stations are indicated.

Bias vs Mean Absolute Error (MAE) for 3 events for 8 ensembles

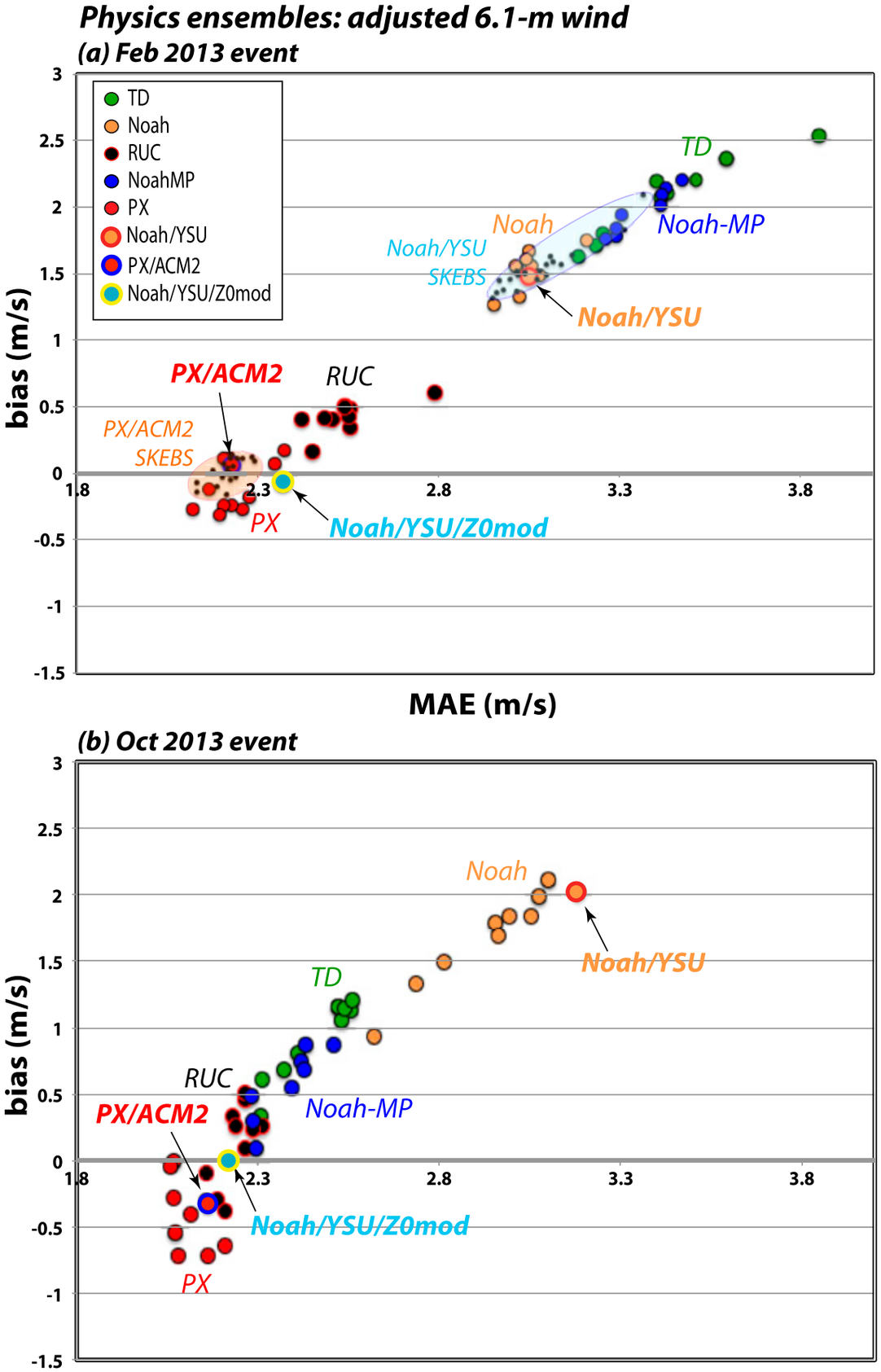

FIG. 6. Scatterplots of network- and event-averaged 6.1-m sustained wind bias vs MAE (both $\mathrm{m\,s^{-1}}$) from the 48 physics ensemble members for the (a) 14–16 Feb 2013, (b) 4–6 Oct 2013, and (c) 13–15 May 2014 episodes, color coded by LSM. Small black dots in (a) show SKEBS perturbation ensemble members made for the PX–ACM2 and Noah–YSU configurations, respectively. Runs PX–ACM2, Noah–YSU, and Noah–YSU–$z_0$mod are marked. For members using the MYJ PBL scheme, the standard but cosmetic recalculation of the near-surface winds was removed (see CF16).

c. *The influence of surface roughness*

Figure 7 summarizes the physics ensemble results with respect to LSM, aggregated over three events (February and October 2013 and May 2014) and representing around 150 simulations in total. The boxplots are based

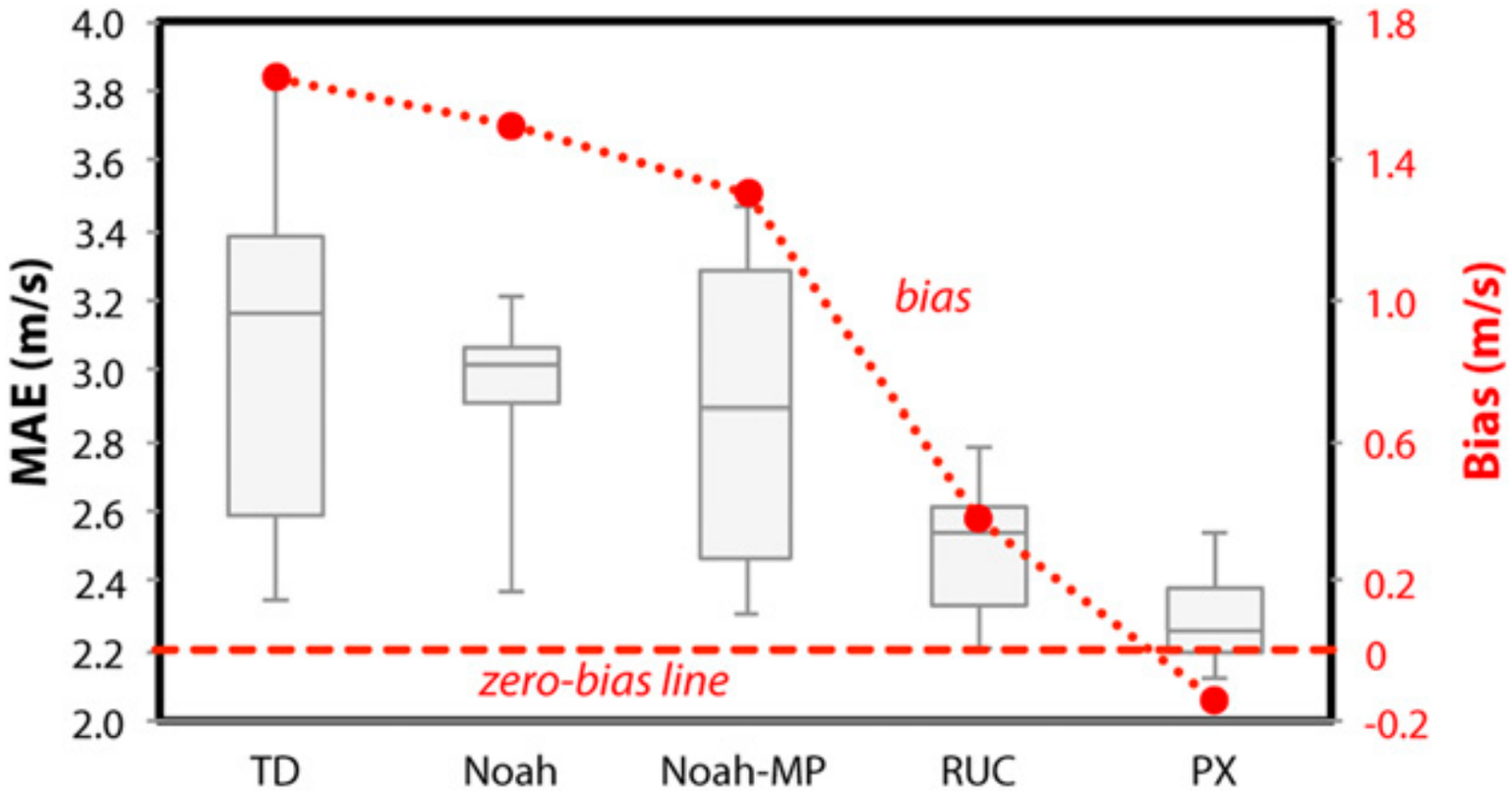

FIG. 7. Boxplots summarizing physics ensemble MAE ($m\,s^{-1}$) distributions stratified by LSM, displaying the median, first quartile, and third quartile values, with the whiskers identifying minima and maxima. The superposed red dotted line depicts their mean biases ($m\,s^{-1}$).

As a test, we modified the Noah LSM to utilize the same surface roughness values of each land-use type employed by PX (Table 2), which meant removing the seasonal cycle and increasing z_0 values for most categories, especially the open and closed shrublands that dominate the San Diego County landscape. The modified Noah simulations, dubbed "Noah–YSU–$z_0$mod" (Fig. 6), were very competitive with respect to event- and network-averaged bias and MAE, with near-to-zero biases and much smaller MAEs (comparable to PX's). Note that the revised Noah LSM also produced a temporally averaged airflow during the jump phase for the February 2013 event (Fig. 3d) that closely resembles that established by PX–ACM2 (Fig. 3a).

TABLE 2. Default roughness lengths (m) employed by land surface schemes for MODIS land-use (LU) categories occurring in the SDG&E network. Water areas of the 2-km nest are excluded.

MODIS LU index	Land fraction (%)	PX	Noah (February)	MODIS (winter)	Noah (October)	Noah (May)	MODIS (summer)	Type
1	8.2	1	0.5	0.5	0.5	0.5	0.5	Evergreen needleleaf forest
2	0.7	0.9	0.5	0.5	0.5	0.5	0.5	Evergreen broadleaf forest
5	11.1	1	0.3	0.2	0.23	0.5	0.5	Mixed forests
6	8.2	0.15	0.03	0.01	0.02	0.05	0.05	Closed shrublands
7	59.2	0.15	0.04	0.01	0.02	0.06	0.06	Open shrublands
8	0.7	0.25	0.05	0.01	0.06	0.05	0.05	Woody savannas
9	0.7	0.15	0.10	0.15	0.1	0.1	0.15	Savannas
10	3.0	0.07	0.1	0.1	0.2	0.1	0.12	Grasslands
13	8.2	0.8	0.5	0.8	0.5	0.5	0.8	Urban

4. Wind forecast bias analysis for individual stations

This section utilizes a composite of six Santa Ana events, adding the 29 April–1 May 2014, 23–25 January 2015, and 11–13 February 2015 events (Table 1) to the three considered for the physics ensemble. Again, each simulation is 54 h long and comparisons with observations were performed hourly, so the composite dataset consisted of 324 observation times, initialization times having been excluded.

Figure 9a shows average forecast wind biases for the composite at the 135 SDG&E stations common to all six events in rank order. As with the similar figure

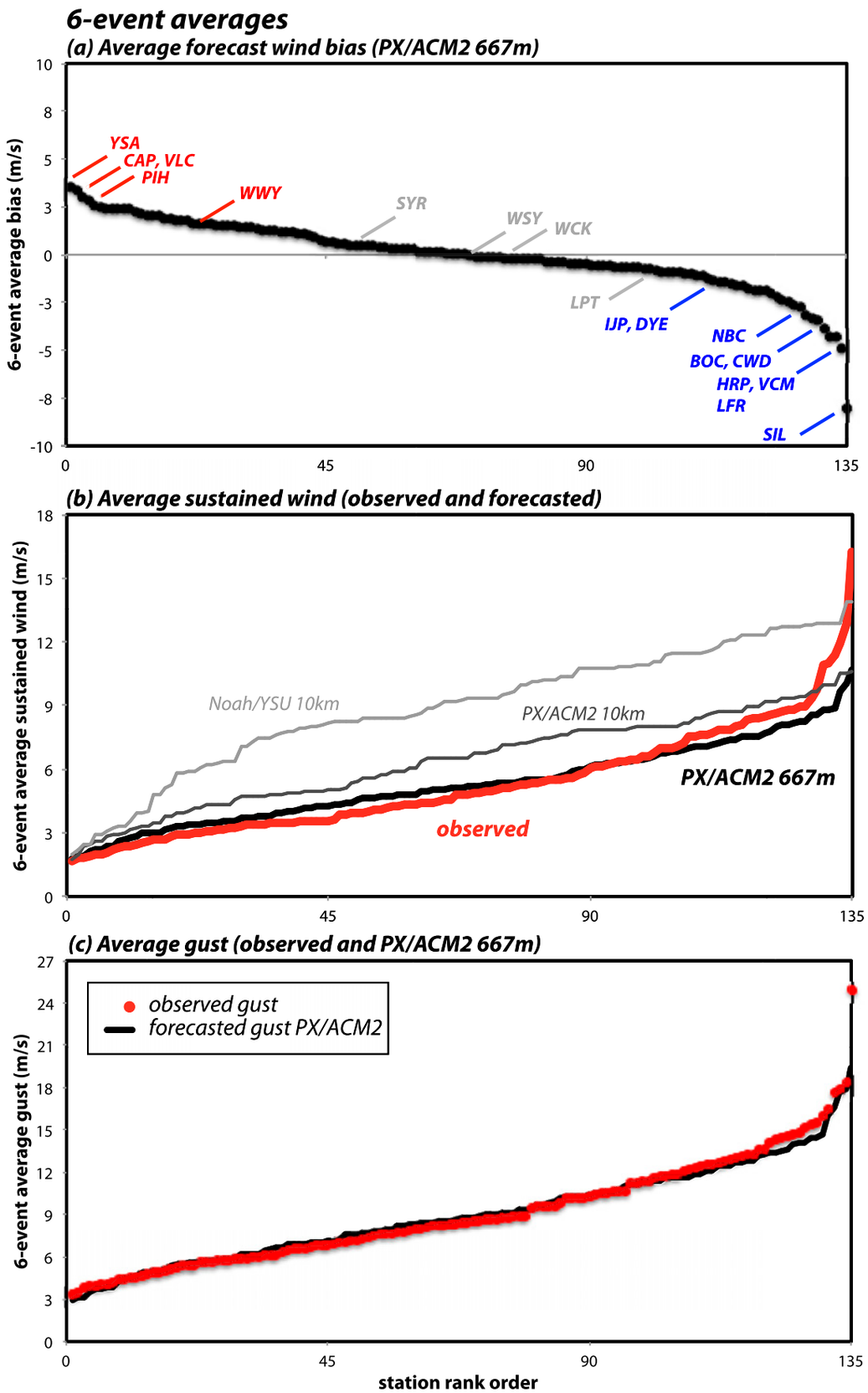

FIG. 9. (a) Sustained wind bias ($m\,s^{-1}$) for PX–ACM2 simulations, (b) sustained winds (red, observed; black, PX–ACM2 667 m; dark gray, PX–ACM2 10 km; and light gray, Noah–YSU 10 km; $m\,s^{-1}$), and (c) gusts (red, observed; black, forecasted using PX–ACM2; $m\,s^{-1}$), all averaged over six Santa Ana events (see Table 1), in station rank order with selected stations identified in (a), color coded by sign of the bias. Only the 135 stations available for all six events are included.

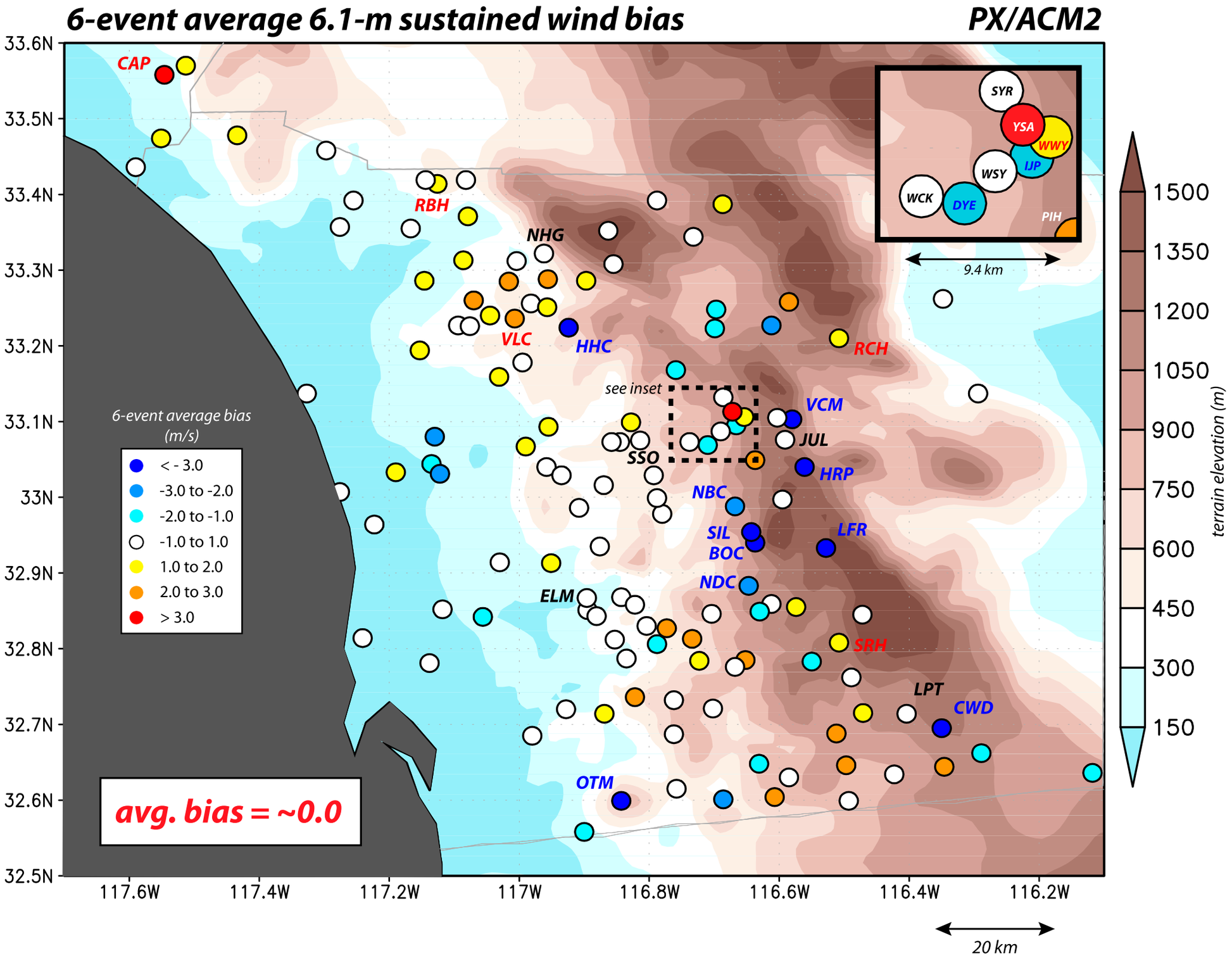

FIG. 10. Spatial distribution of six-event-average 6.1-m sustained wind bias ($m\,s^{-1}$), color coded as indicated. The average bias over the entire SDG&E network is around $0\,m\,s^{-1}$. Inset shows the subset of the 135 stations in the Santa Ysabel vicinity. The locations of stations mentioned by name in the text and/or figures are identified.

5. A gust parameterization for the SDG&E network and its stations

Numerical models of the present type do not resolve short-period (~3 s) gusts, because they cannot directly capture the turbulent motions that these wind bursts represent. This is true even if the model employs a time step on the order of a few seconds, as model filters will still act to suppress variations with time scales of less than several minutes. Because of this, it is most sensible to compare model outputs to observed sustained winds and construct a reasonable gust parameterization. In this section, we pursue a simple gust model for individual stations and the SDG&E mesonet as a whole.

a. Station wind and gust predictions

Figure 12a presents the relationship between observed sustained winds and gusts for the six-event composite dataset, each point representing an SDG&E station's values after averaging over the 324 hourly observations. The no-intercept least squares fit to the entire dataset yields a slope (or GF) of 1.7 with an R^2 of 0.89. This suggests that adequate forecasts of sustained winds could result in skillful predictions of observed gusts in a simple manner via a constant gust factor, that being 1.7 in the present example. The relationship

As a consequence, *biased* forecasts for the observed sustained winds can be used to make *unbiased* estimates of the observed gusts. This is demonstrated in Figs. 12d and 9c, which now plot forecasted versus observed gusts.

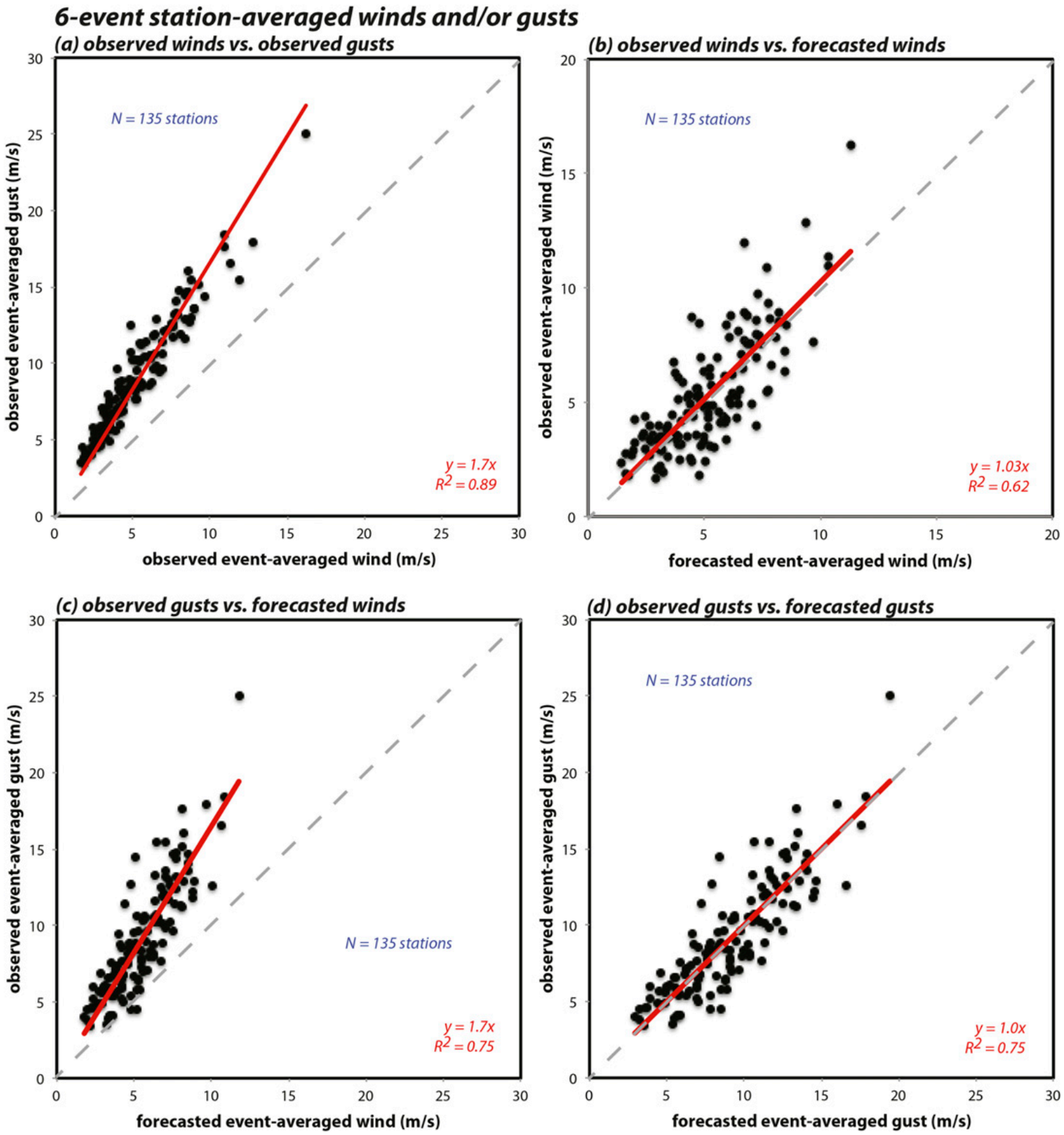

FIG. 12. Scatterplots of six-event-mean (a) observed event-averaged sustained wind vs observed event-averaged gust, (b) observed event-averaged sustained wind vs forecasted event-averaged sustained wind, (c) forecasted event-averaged sustained wind vs observed event-averaged gust, and (d) observed event-averaged gust vs forecasted event-averaged gust using a gust factor of 1.7 for the 135 SDG&E stations. Each dot represents a station. A zero-intercept least squares fit (red line) and the 1:1 line (dashed gray) are shown in each panel for reference, with slopes and R^2 values indicated. (All units are m s^{-1}.)

As a consequence, *biased* forecasts for the observed sustained winds can be used to make *unbiased* estimates of the observed gusts. This is demonstrated in Figs. 12d and 9c, which now plot forecasted versus observed gusts. The gust predictions were made by multiplying the sustained wind prediction for each site by a single, constant GF of 1.7, as suggested by Fig. 12c. There are

Network-averaged winds and/or gusts

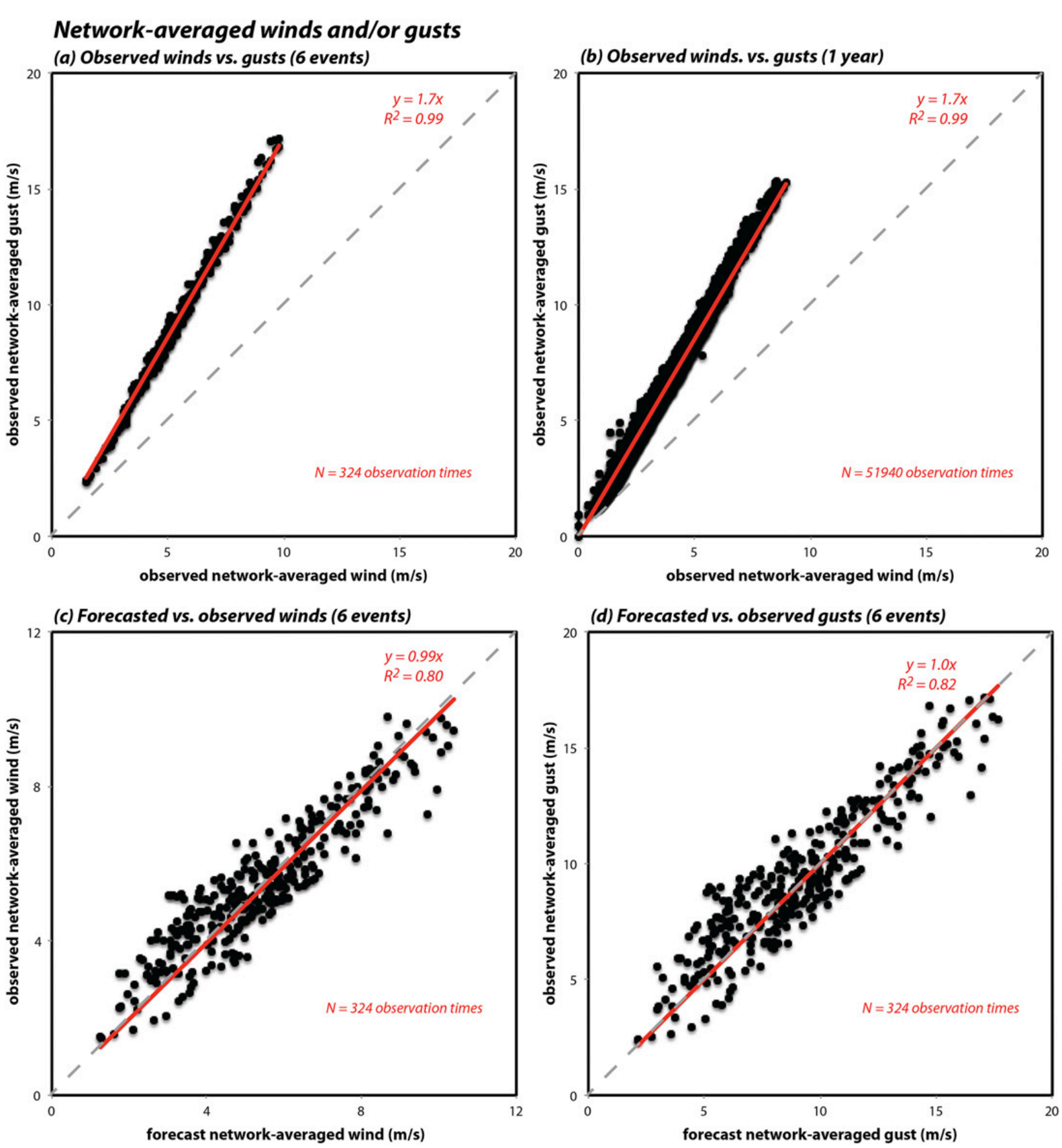

FIG. 13. Scatterplots of network-averaged (a) observed wind vs observed gust over the six events (324 observation times), (b) observed wind vs observed gust for 1 yr (51 940 observation times), (c) observed wind vs forecasted wind over the six events, and (d) observed gust vs forecasted gust over the six events. Each dot is a network average based on 135 SDG&E stations. A zero-intercept least squares fit (red line) and the 1:1 line (dashed gray) are shown in each panel for reference, with slopes and R^2 values indicated. (All units are $\mathrm{m\,s^{-1}}$.)

Finally, we apply this constant GF concept to make predictions of network-averaged gusts for individual Santa Ana wind events. Figure 14 presents time series of the observed (dotted lines) and forecasted (solid lines) winds (black) and gusts (red) over the SDG&E mesonet for the six Santa Ana episodes. Generally, the gust parameterization captures the amplitude and temporal evolution of the gusts for all six of the events quite well, especially the peaks. Obviously, performance depends upon the sustained wind predictions being correct in the first place. Gust over-

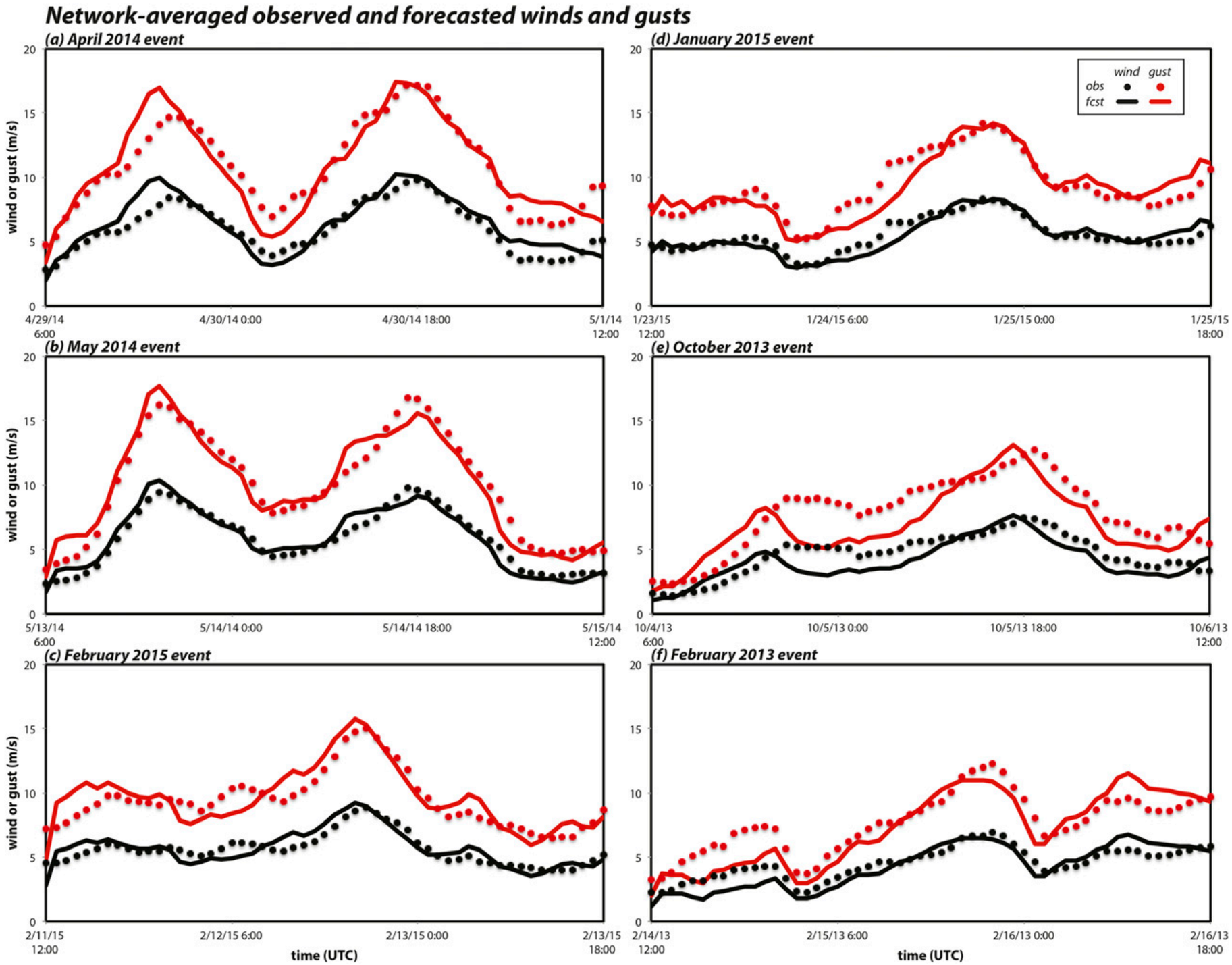

FIG. 14. Time series of network-averaged observed (black dots) and predicted (red curves) 6.1-m sustained winds (black; m s^{-1}) and gusts (red; m s^{-1}) for the (a) April 2014, (b) May 2014, (c) February 2015, (d) January 2015, (e) October 2013, and (f) February 2013 events (see Table 1). The GF used to forecast gusts is 1.7, based on the network-averaged wind vs the network-averaged gust.

6. Discussion and summary

We seek to obtain skillful gust forecasts in San Diego County during Santa Ana wind events. These hazard (Rolinski et al. 2016). As models of the present type cannot resolve gusts, this effort must start with making sure sustained wind predictions are as accurate as possible and then deducing gusts via an algorithm or parameterization of some kind. We attempted to partition the forecast sustained wind bias into "fixable" and "unavoidable" components. The fixable part may be addressed via the model configuration, including refinements of physical parameterizations, among many other things, leaving the unavoidable portion to be mitigated via postprocessing.

Even a model configuration that yielded negligible bias when averaged over multiple events and stations was still found to possess systematic errors at individual sites. These errors were shown to be inversely correlated with the average observed wind: the model tended to overpredict locales with weaker winds while underpredicting speeds where measured winds were stronger. Forecast sustained wind speed bias was also seen to be correlated with, and proportional to, the observed gust factor (GF), the ratio of the observed sustained wind and gust. This is mainly true since the GF and sustained wind are (negatively) correlated: sites with larger GFs tend to have slower winds.

We interpreted the difference between a given station's GF and the network average (1.7 for the SDG&E mesonet as a whole, with virtually no scatter or weather dependence) as a measure of very localized anemometer exposure that cannot be captured even at reasonably high spatial resolution and, thus, an unavoidable component of the bias. Sites with obstacles or landforms that tend to slow the temporally averaged sustained wind more than the transient, impulsive gusts would result in GFs that are larger than the network average, and its winds would be more likely to be overpredicted. In contrast, stations having local features that help enhance the winds relative to the gusts would have lower GFs and be underpredicted. In practice, both were found to be the case, as after using the observed GF to predict sustained wind forecast bias, the remainder of the bias was independent of observed wind speeds.

The gust algorithm that emerged from this study is extremely simple: we multiply sustained wind forecasts at each site by the network average GF of 1.7. Gust

My review of this paper

- The goals are clearly stated.
- The methods are clearly described.
- The results are well-presented graphically.
- The conclusions are well-supported by their results.
- The study is a valuable contribution to mesoscale forecasting of Santa Ana wind speeds and gusts.
- The study nicely demonstrates how model physics (LSMs in this case) can be evaluated using observations.
- The study is also an example of using observations (from a dense mesonet in this case) to extend what a mesoscale model can skillfully predict (wind speeds), by relating gusts (not resolvable by model) to model-predicted wind speeds.